Limits of Offshore wind energy - database of energy production of offshore wind farms in the Baltic, North and Irish Seas, and model validation

Carlos Simao Ferreira

*Faculty Aerospace Engineering, Delft University of Technology.

Corresponding author(s). E-mail(s): c.j.simaoferreira@tudelft.nl;

Abstract

Offshore wind energy is increasingly recognized as a crucial resource for coastal regions, offering significant potential for sustainable energy development. However, the spatial constraints in marine environments often necessitate high-density wind farm configurations, which can adversely affect overall wind farm efficiency. This database provides the production data for over seventy offshore wind farms located in the Baltic, North, and Irish Seas, collected from public data. The data is used to validate widn farm produciton models. This study explores the limits of offshore wind energy by focusing on the relationship between wind farm power density and efficiency, specifically examining how high-density installations influence capacity factors. The work introduces a novel perspective by asserting that the maximum capacity factor is primarily dictated by the wind farm's wind factor—a measure of environmental and operational conditions. Utilizing a closed-form analytical model, we calculated the average annual production for all the widn farms. The findings indicate that the capacity factors of these wind farms adhere to and are constrained by a theoretical limit as a function of the wind farm's wind factor. Most wind farms are already performing at around 90% of the theoretical maximum. The implications of this relationship are critical for future offshore wind farm planning and deployment, suggesting a need for strategic considerations regarding farm density to maximize energy output and minimize curtailment risks. This study develops case studies that demonstrate how these dynamics impose significant limits on the development ambitions of offshore wind energy. An extended work is to be published with the participation of additional authors.

1 Wind Farm data

1.1 Wind Farm Data Collection

The wind farm data for this study were collected from a variety of public, verifiable sources to ensure a comprehensive dataset covering 72 offshore wind farms (71 are listed in Table 1, as the two Trianel wind farms are analyzed as one.). The data for each wind farm was collected from multiple platforms, including industry reports, renewable energy databases, government and regulator publications, and study reports (e.g. see [1–5]). The data sources for the estimation of the capacity factor, including the years considered, are also presented in Table 1. For wind farms with several wind turbine models, an equivalent power and diameter was considered with a insptalled-capacity weighted average that preserves total loading and power density. The location of the wind farms is shown in Figure 1. Figure 2 shows the distribution of wind farm size in MW and wind farm density MW/km^2 of the dataset, where the size of the marker is proportional to the size of the rotor.

The primary parameters collected for each wind farm included the installed capacity (in megawatts, MW), the area covered by the wind farm (in square kilometers, km^2), the number of wind turbines, the rated power of each turbine (MW), the diameter of the rotor D (in meters, m), and the height of the nacelle h (in meters, m). For each wind farm location, the unperturbed average wind speed at a given reference height (h_w) was retrieved from [6]. The wind distribution is assumed to follow a Weibull distribution, with shape parameter $k_w = 2.4$ assumed representative for all locations [7]. With this assumption, we determine the scale parameter λ_w for each location from the annual mean wind speed. The simulations assume a surface roughness $z_0 = 10^{-5}m$. The power coefficient and thrust coefficient at below rated wind speed are assumed to be the same for all turbines $C_P = 0.46$ and $C_P = 0.75$.

An Excel file with the data provided in Table 1 is available in the repository.

1.2 List of Wind Farms

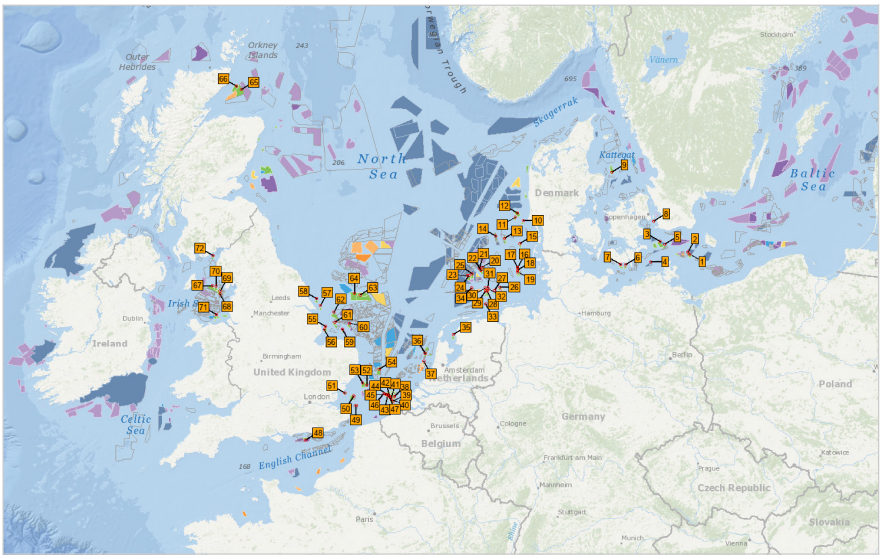

Fig. 1 Map of location of wind farms in the Baltic, North and Irish Seas. Labels follow the indexes in Table 1. The background of the figure is adapted from [8].

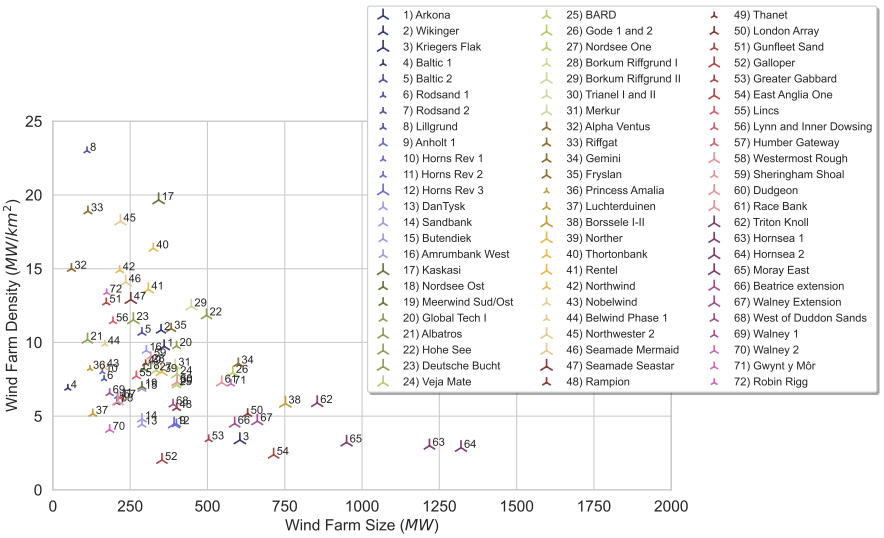

Fig. 2 Distribution of wind farm size in MW and wind farm density MW/km^2 of the dataset. The size of the marker is proportional to the size of the rotor. Labels follow the indexes in Table 1.

Table 1: Wind Farm Data Summary

	Name	Country	Installed capacity (MW)	Installed density (MW/km^2)	Wind farm area (km^2)	Number of wind turbines	Wind Turbine rated power (MW)	Wind Turbine rotor diameter (m)	Wind Turbine nacelle height, (m)	Wind λ_w, (m/s)	Wind k_w	Wind h_w, (m)	Capacity Factor (CF), real data (%)	CF, model (%)	CF, model infinite farm (%)	CF, model isolated turbine (%)	Years of data	Sources of data	Model parameter M_{rows}	Model parameter $M_{turbines}$
1	Arkona	DE	360.0	9.7	37.0	60	6.0	154.0	102.0	10.8	2.4	100	41.0	45.6	34.6	61.1	2019-2023	[9]	2.5	10.0
2	Wikinger	DE	350.0	10.8	32.3	70	5.0	135.0	97.5	10.8	2.4	100	38.9	40.4	31.5	59.1	2019-2023	[10–12]	2.5	9.0
3	Kriegers Flak	DK	604.8	3.4	179.0	72	8.4	167.0	107.0	11.0	2.4	100	44.2	51.6	46.2	59.0	2022-2023	[13]	2.5	12.0
4	Baltic 1	DE	48.3	6.9	7.0	21	2.3	93.0	67.0	10.8	2.4	100	42.6	55.0	37.7	58.5	2016-2023[1]	[10–12]	2.5	7.0
5	Baltic 2	DE	288.0	10.7	27.0	80	3.6	120.0	78.2	10.8	2.4	100	42.6	44.5	30.3	60.6	2016-2023	[10–12]	2.5	15.0
6	Rodsand 1	DK	165.6	7.5	22.0	72	2.3	82.0	69.0	10.8	2.4	100	35.6	40.1	31.1	52.8	2010-2023	[13]	2.5	12.0
7	Rodsand 2	DK	207.0	5.9	35.0	90	2.3	93.0	68.0	10.8	2.4	100	43.0	48.4	36.7	58.9	2011-2023	[13]	2.5	19.0
8	Lillgrund	SE	110.4	23.0	4.8	48	2.3	93.0	65.0	10.5	2.4	100	31.0	35.2	16.6	56.4	2010-2023	[14]	2.5	9.0
9	Anholt 1	DK	399.6	4.5	89.4	111	3.6	120.0	81.6	11.0	2.4	100	48.5	52.4	43.2	62.0	2014-2023	[13]	2.5	21.9
10	Horns Rev 1	DK	160.0	8.0	20.0	80	2.0	80.0	70.0	11.5	2.4	100	39.7	46.7	35.5	59.4	2010-2023	[13]	2.5	15.0
11	Horns Rev 2	DK	209.3	6.3	33.0	91	2.3	93.0	68.0	11.5	2.4	100	46.6	51.8	39.8	62.8	2010-2023	[13]	2.5	19.0
12	Horns Rev 3	DK	392.0	4.5	88.0	49	8.0	164.0	112.0	11.5	2.4	100	49.4	56.0	47.9	62.4	2020-2023	[13]	2.5	11.0
13	DanTysk	DE	288.0	4.4	64.9	80	3.6	120.0	88.0	11.3	2.4	100	47.6	54.6	46.3	64.0	2016-2022	[9]	2.5	15.0
14	Sandbank	DE	288.0	4.8	60.0	72	4.0	130.0	94.8	11.4	2.4	100	48.9	57.0	47.3	65.7	2018-2022	[9]	2.5	15.2
15	Butendiek	DE	288.0	6.9	42.0	80	3.6	120.0	91.0	11.3	2.4	100	46.7	51.0	41.0	63.9	2018, 2020, 2022	[15–19]	2.5	14.0
16	Amrumbank West	DE	302.4	9.4	32.0	80	3.8	120.0	90.0	11.2	2.4	100	40.0	48.2	35.5	62.5	2016-2022	[9]	2.5	15.0
17	Kaskasi	DE	342.0	19.7	17.4	38	9.0	167.0	107.5	11.2	2.4	100	31.2	35.2	26.8	58.7	2023Q2-2024Q1	[9]	2.5	4.0
18	Nordsee Ost	DE	295.2	8.2	36.0	48	6.2	126.0	92.0	11.2	2.4	100	33.6	38.3	34.3	53.8	2016-2022	[9]	2.5	4.0
19	Meerwind Sud/Ost	DE	288.0	7.0	41.1	80	3.6	120.0	89.0	11.2	2.4	100	43.2	48.9	40.1	63.5	2022-2022	[15]	2.5	12.0

Continued on next page

[1]For Baltic 1 and 2, the data represents the total of both wind farms.

Table 1 – continued from previous page

	Name	Country	Installed capacity (MW)	Installed density (MW/km^2)	Wind farm area (km^2)	Number of wind turbines	Wind Turbine rated power (MW)	Wind Turbine rotor diameter (m)	Wind Turbine nacelle height, (m)	Wind λ_w, (m/s)	Wind k_w	Wind h_w, (m)	Capacity Factor (CF), real data (%)	CF, model (%)	CF, model infinite farm (%)	CF, model isolated turbine (%)	Years of data	Sources data	Model parameter M_{rows}	Model parameter $M_{turbines}$
20	Global Tech I	DE	400.0	9.8	41.0	80	5.0	116.0	82.0	11.2	2.4	100	34.4	36.0	30.9	54.4	2022-2022	[15]	2.5	7.0
21	Albatros	DE	112.0	10.2	11.0	16	7.0	154.0	105.0	11.2	2.4	100	40.2	46.1	39.5	60.7	2020-2023	[9]	2.5	2.0
22	Hohe See	DE	497.0	11.8	42.0	71	7.0	154.0	105.0	11.2	2.4	100	37.6	41.9	33.2	60.7	2020-2023	[9]	2.5	9.0
23	Deutsche Bucht	DE	260.4	11.5	22.6	31	8.4	167.0	100.0	11.2	2.4	100	42.8	49.0	34.7	59.9	2020-2023[2]	[20–24]	2.5	7.0
24	Veja Mate	DE	402.0	7.9	51.2	67	6.0	154.0	103.3	11.2	2.4	100	42.8	45.7	40.4	63.9	2020-2022	[25]	2.5	6.0
25	BARD	DE	400.0	7.1	56.3	80	5.0	122.0	90.0	11.2	2.4	100	37.8	40.6	36.8	57.1	2018-2023	[1, 9]	2.5	6.0
26	Gode 1 and 2	DE	582.0	7.9	73.3	97	6.0	154.0	104.0	11.2	2.4	100	38.1	44.3	39.2	63.6	2017-2023	[9]	2.5	8.0
27	Nordsee One	DE	334.8	8.1	41.3	54	6.2	126.0	90.0	11.2	2.4	100	37.0	41.8	33.6	53.2	2019-2023[3]	[20–24]	2.5	9.0
28	Borkum Riffgrund I	DE	312.0	8.7	36.0	78	4.0	120.0	83.0	11.2	2.4	100	33.5	37.2	35.5	61.1	2018-2023	[9]	2.5	2.0
29	Borkum Riffgrund II	DE	448.0	12.4	36.0	56	8.0	164.0	105.0	11.2	2.4	100	33.3	44.0	32.9	60.5	2019-2023	[9]	2.5	9.0
30	Trianel I and II	DE	401.6	7.2	55.6	72	5.6	133.2	90.0	11.2	2.4	100	34.3	42.3	37.5	58.7	2020-2022[4]	[26–28]	2.5	6.5
31	Merkur	DE	396.0	8.4	47.0	66	6.0	150.0	100.0	11.2	2.4	100	41.5	43.1	38.6	62.7	2021-2023	[29–32]	2.5	5.0
32	Alpha Ventus	DE	60.0	15.0	4.0	12	5.0	121.0	92.0	11.2	2.4	100	35.4	38.0	33.0	56.9	2022-2022	[15]	2.5	1.0
33	Riffgat	DE	113.4	18.9	6.0	30	3.8	120.0	90.0	11.0	2.4	100	37.4	46.8	26.4	61.3	2022-2022	[15]	2.5	7.0
34	Gemini	NL	600.0	8.6	70.0	150	4.0	130.0	89.0	11.2	2.4	100	45.5	49.0	36.9	64.7	2019-2023	[20–24]	2.5	26.0
35	Fryslan	NL	382.7	10.9	35.0	89	4.3	130.0	115.0	10.7	2.4	100	37.7	42.6	33.1	61.2	2022-2023	[33]	2.5	12.0
36	Princess Amalia	NL	120.0	8.2	14.6	60	2.0	80.0	80.0	10.6	2.4	100	43.0	41.8	31.3	54.3	2016-2018	[34–36]	2.5	11.0
37	Luchterduinen	NL	129.0	5.2	25.0	43	3.0	112.0	81.0	10.6	2.4	100	43.0	52.3	40.9	60.4	2016-2018	[34–36]	2.5	10.0
38	Borssele I-II	NL	752.0	5.9	128.3	94	8.0	167.0	116.0	10.6	2.4	100	41.0	43.2	39.2	57.9	2021-2023[5]	[38–42]	2.5	8.0

Continued on next page

[2]Includes GWh produced as well as attributed to paid curtailments ([20–24]).
[3]Includes GWh produced as well as attributed to paid curtailments ([20–24]).
[4]Data of both widn farms is agregated, as the two wind farms are intertwined.
[5]MWh determined from the Renewable Energy Guarantees of Origin (REGO) certificates issued [37].

Table 1 – continued from previous page

	Name	Country	Installed capacity (MW)	Installed density (MW/km^2)	Wind farm area (km^2)	Number of wind turbines	Wind Turbine rated power (MW)	Wind Turbine rotor diameter (m)	Wind Turbine nacelle height, (m)	Wind λ_w, (m/s)	Wind k_w	Wind h_w, (m)	Capacity Factor (CF), real data (%)	CF, model (%)	CF, model infinite farm (%)	CF, model isolated turbine (%)	Years of data	Sources data	Model parameter M_{rows}	Model parameter $M_{turbines}$
39	Norther	BE	352.0	8.0	44.0	44	8.0	164.0	98.0	10.6	2.4	100	38.6	42.1	34.7	56.3	2020-2023	[9]	2.5	6.0
40	Thortonbank	BE	325.0	16.4	19.8	54	6.0	126.0	95.0	10.6	2.4	100	32.9	36.9	22.8	50.4	2015-2023	[9]	2.5	11.0
41	Rentel	BE	308.7	13.6	22.7	42	7.4	154.0	119.0	10.6	2.4	100	35.5	39.1	29.6	56.2	2019-2023	[9]	2.5	6.0
42	Northwind	BE	216.0	14.9	14.5	72	3.0	112.0	71.0	10.6	2.4	100	38.0	39.9	23.6	59.8	2015-2023	[9]	2.5	13.0
43	Nobelwind	BE	165.0	8.3	19.8	50	3.3	112.0	79.0	10.6	2.4	100	39.8	43.2	33.1	58.2	2018-2023	[9]	2.5	8.0
44	Belwind Phase 1	BE	168.0	9.9	17.0	56	3.0	90.0	72.0	10.6	2.4	100	33.4	35.9	26.6	49.7	2015-2023	[9]	2.5	9.0
45	Northwester 2	BE	218.5	18.2	12.0	23	9.5	164.0	105.0	10.6	2.4	100	31.5	34.1	25.2	52.6	2021-2023	[9]	2.5	3.0
46	Seamade Mermaid	BE	235.2	14.1	16.7	28	8.4	167.0	109.0	10.6	2.4	100	38.1	44.0	29.6	56.5	2021-2023	[9]	2.5	6.0
47	Seamade Seastar	BE	252.0	12.9	19.5	30	8.4	167.0	109.0	10.6	2.4	100	34.7	39.2	30.6	56.5	2021-2023	[9]	2.5	4.0
48	Rampion	UK	400.2	5.6	72.0	116	3.4	116.0	80.0	10.6	2.4	100	42.3	44.5	37.1	58.5	2020-2023[6]	[37]	2.5	16.0
49	Thanet	UK	300.0	8.6	35.0	100	3.0	90.0	70.0	10.6	2.4	100	32.8	36.7	27.1	49.6	2011-2023	[37]	2.5	17.0
50	London Array	UK	630.0	5.2	122.0	175	3.6	120.0	87.0	10.6	2.4	100	40.7	44.7	38.7	59.5	2014-2023	[37]	2.5	20.0
51	Gunfleet Sand	UK	172.8	12.7	13.6	48	3.6	107.0	75.0	10.6	2.4	100	35.5	38.9	25.6	54.0	2011-2023		2.5	9.0
52	Galloper	UK	352.8	2.0	174.0	56	6.3	154.0	103.0	10.7	2.4	100	46.0	52.4	50.3	59.8	2019-2023	[37]	2.5	5.0
53	Greater Gabbard	UK	504.0	3.4	147.0	140	3.6	107.0	77.5	10.7	2.4	100	40.2	43.3	40.2	54.6	2013-2023	[37]	2.5	12.0
54	East Anglia One	UK	714.0	2.4	300.0	102	7.0	154.0	90.0	10.8	2.4	100	45.3	50.4	46.1	57.1	2021-2023	[37]	2.5	16.0
55	Lincs	UK	270.0	7.7	35.0	75	3.6	120.0	100.0	11.0	2.4	100	41.3	45.2	38.8	62.8	2014-2022	[37]	2.5	8.0
56	Lynn and Inner Dowsing	UK	194.4	11.4	17.0	54	3.6	107.0	80.0	11.0	2.4	100	34.9	39.7	29.6	56.8	2010-2023	[37]	2.5	8.0
57	Humber Gateway	UK	219.0	6.3	35.0	73	3.0	112.0	80.0	11.1	2.4	100	42.7	48.4	40.6	63.4	2016-2023	[37]	2.5	10.0
58	Westermost Rough	UK	210.0	6.0	35.0	35	6.0	154.0	100.0	11.1	2.4	100	47.5	55.0	44.1	63.1	2017-2023	[37]	2.5	8.0
59	Sheringham Shoal	UK	316.8	9.1	35.0	88	3.6	107.0	80.0	11.0	2.4	100	37.9	43.2	31.8	56.8	2013-2023	[37]	2.5	16.0

Continued on next page

[6]MWh determined from the Renewable Energy Guarantees of Origin (REGO) certificates issued [37].

Table 1 – continued from previous page

	Name	Country	Installed capacity (MW)	Installed density (MW/km^2)	Wind farm area (km^2)	Number of wind turbines	Wind Turbine rated power (MW)	Wind Turbine rotor diameter (m)	Wind Turbine nacelle height, (m)	Wind λ_w, (m/s)	Wind k_w	Wind h_w, (m)	Capacity Factor (CF), real data (%)	CF, model (%)	CF, model infinite farm (%)	CF, model isolated turbine (%)	Years of data	Sources data	Model parameter M_{rows}	Model parameter $M_{turbines}$
60	Dudgeon	UK	402.0	7.3	55.0	67	6.0	154.0	110.0	11.0	2.4	100	45.6	50.9	40.9	63.2	2018-2023	[37]	2.5	12.0
61	Race Bank	UK	546.0	7.3	75.0	91	6.0	154.0	100.0	11.1	2.4	100	43.6	49.4	39.8	63.1	2019-2023	[37]	2.5	15.0
62	Triton Knoll	UK	855.0	5.9	145.0	90	9.5	164.0	105.0	11.1	2.4	100	40.2	46.3	38.7	55.9	2023-2023	[37]	2.5	16.0
63	Hornsea 1	UK	1218.0	3.0	407.0	174	7.0	154.0	113.0	11.2	2.4	100	45.4	52.2	48.6	61.0	2020-2023	[37]	2.5	20.0
64	Hornsea 2	UK	1320.0	2.9	462.0	165	8.0	164.0	118.0	11.2	2.4	100	42.2	52.1	49.3	61.0	2023-2023	[37]	2.5	16.0
65	Moray East	UK	950.0	3.2	295.0	100	9.5	164.0	105.0	11.4	2.4	100	40.5	49.6	46.1	57.7	2022-2022[7]	[37]	2.5	12.0
66	Beatrice extension	UK	588.0	4.5	131.0	84	7.0	154.0	100.0	11.1	2.4	100	43.5	49.7	43.5	59.5	2020-2023[8]	[37]	2.5	13.0
67	Walney Extension	UK	661.2	4.7	142.0	87	7.6	159.0	115.5	11.2	2.4	100	45.2	50.5	44.6	60.3	2019-2023[9]	[37]	2.5	13.0
68	West of Duddon Sands	UK	388.8	5.8	67.0	108	3.6	120.0	90.0	11.2	2.4	100	44.3	47.8	41.9	63.2	2015-2023	[37]	2.5	12.0
69	Walney 1	UK	183.6	6.6	28.0	51	3.6	107.0	83.5	11.2	2.4	100	39.0	42.0	38.2	57.9	2012-2023	[37]	2.5	4.0
70	Walney 2	UK	183.6	4.1	45.0	51	3.6	120.0	90.0	11.2	2.4	100	44.2	51.1	47.2	63.2	2012-2023	[37]	2.5	5.0
71	Gwynt y Môr	UK	576.0	7.2	80.0	160	3.6	107.0	98.0	10.8	2.4	100	34.1	37.4	34.7	56.4	2016-2023	[37]	2.5	8.0
72	Robin Rigg	UK	174.0	13.4	13.0	58	3.0	90.0	98.0	10.6	2.4	100	35.5	38.9	25.7	51.3	2011-2023	[37]	2.5	12.0

[7]Production data is adjusted to compensate a 23.5% loss due to curtailement from 2021/2022, as quantified in [**?**]
[8]Production data is adjusted to compensate a 16% loss due to curtailement from 2021/2022, as quantified in [**?**]
[9]Production data is adjusted to compensate a 5% loss due to curtailement from 2021/2022, as quantified in [**?**]

1.3 Wind farm model description

The model for wind farm production is adapted from the model presented by [43, 44], building upon the wind farm wake models by [45] and [46].

1.3.1 Wind turbine model description

The model estimates the power production of a wind turbine based on the wind speed it encounters. It includes mathematical formulations for calculating the power output at varying wind speeds, accounting for both below and above the rated wind speed of the turbine.

$$P(U) = \alpha U^3 + \beta \tag{1}$$

Equation 1 describes the power production of a wind turbine as a function of the wind speed U for below rated conditions, where α and β are coefficients that depend on the turbine's specifications and operational settings as defined in Equation 2 as

$$\alpha = \frac{P_G}{U_r^3 - U_{in}^3}, \quad \beta = -\frac{P_G U_{in}^3}{U_r^3 - U_{in}^3} \tag{2}$$

In Equation 2, P_G is the rated (installed) generator power, U_{in} is the cut-in wind speed, and U_r is the rated wind speed. The coefficients α and β determine the curve's shape, affecting how the turbine's power output scales with wind speed.

$$C_T \equiv \frac{T}{\rho A_R U^2}, \quad C_P \equiv \frac{P}{\rho A_R U^3} \tag{3}$$

Equation 3 defines the thrust coefficient C_T and power coefficient C_P, which are critical in determining the aerodynamic forces acting on the turbine blades and the efficiency of power generation, respectively.

$$U_r = \sqrt[3]{\frac{8 P_G}{\rho \pi D^2 C_{P,\text{rated}}}} \tag{4}$$

Equation 4 computes the rated wind speed U_r from the turbine specifications, including the air density ρ, rotor diameter D, and the rated power coefficient $C_{P,\text{rated}}$.

$$P(U) = \begin{cases} \alpha U^3 + \beta & \text{for } U_{in} \leq U < U_r \\ P_G & \text{for } U_r \leq U \leq U_{out} \end{cases} \tag{5}$$

Equation 5 provides a piecewise definition of the turbine's power curve. Below the rated wind speed (U_r), the power output increases with the cube of the wind speed. Above this speed, the turbine produces a constant power P_G, which is the maximum generator capacity, until the cut-out wind speed U_{out} is reached.

Equation 6 describes the behavior of the thrust coefficient C_T across different wind speeds. At wind speeds below the rated wind speed, C_T remains constant. Above the rated wind speed, C_T decreases as the cube root of the square of the ratio of the rated

wind speed to the actual wind speed, reflecting changes in aerodynamic loading on the turbine blades.

$$C_T = \begin{cases} C_{T,\text{rated}} & \text{for } U_{in} \leq U < U_r \\ C_{T,\text{rated}} \left(\frac{U_r}{U}\right)^{3.2} & \text{for } U_r \leq U \leq U_{out} \end{cases} \tag{6}$$

1.3.2 Wind Farm topology model

The model simplifies wind farm topology effects into wind farm density, where the only inputs are the total number of turbines N_T and wind farm area A. The topology further simplified by assuming uniform distance between turbines, which allows us to define the dimensionless spacing ratio S (Equation 7).

$$S = \frac{\sqrt{A}}{D\left(\sqrt{N_T} - 1\right)} \tag{7}$$

1.3.3 Wind farm velocity model

The presence of the wind farm adds loading to the lower region of the Atmospheric Boundary Layer, changing the velocity profile. In this section, we present the model for the velocity at hub height in the infinite wind farm as derived by [45–47]. The model assumes that:

- The velocity profile is logarithmic and continuous along the height.
- The wind is infinite, meaning it is large enough for the vertical wind profile to be horizontally homogeneous.
- The horizontally homogeneous vertical wind profile is logarithmic both below and above hub height.
- The height of the planetary boundary layer is considerably larger than the wind turbine hub height.
- Turbulent wind speed fluctuations are horizontally homogeneous.

$$\begin{aligned} U_{\text{lo}}(z) &= \frac{u_{*\text{lo}}}{\kappa} \ln\left(\frac{z}{z_{0,\text{lo}}}\right) \quad \text{for } z < h, \\ U_{\text{hi}}(z) &= \frac{u_{*\text{hi}}}{\kappa} \ln\left(\frac{z}{z_{0,\text{hi}}}\right) \quad \text{for } z > h, \end{aligned} \tag{8}$$

Equation 8 defines the adjusted logarithmic wind profile within a wind farm, taking into account the lower and upper boundary layers (in relation to hub height) affected by wind farm loading. It models the wind speed at different heights, distinguishing between the conditions below and above the turbine hub height h, where the friction velocities u^*_{lo} and u^*_{hi} represent the turbulent stress related to surface roughness $z_{0,\text{lo}}$ and $z_{0,\text{hi}}$.

$$U_{\text{lo}}(h) = U_{\text{hi}}(h) \Rightarrow u^*_{\text{hi}} \ln\left(\frac{h}{z_{0,\text{hi}}}\right) = u^*_{\text{lo}} \ln\left(\frac{h}{z_{0,\text{lo}}}\right) \tag{9}$$

Equation 9 ensures continuity at hub height, which is critical for modeling the transition of wind speeds across the boundary layer at the turbine hub height.

The friction velocity is per definition given as $u^* = \sqrt{\tau_w/\rho}$where $\sqrt{\tau_w}$ is the friction stress at the wall.

$$\tau_{hi} - \tau_{lo} = \rho {u^*_{\text{hi}}}^2 - \rho {u^*_{\text{lo}}}^2 = \frac{\pi}{8} \frac{\rho D^2 U_h^2 C_T}{S^2 D^2} = \rho c_t U_h^2 \tag{10}$$

Equation 10 addresses the conservation of momentum above and below the hub height, incorporating the turbine's thrust as a key factor. It quantifies the difference in momentum between the upper and lower boundary layers due to the thrust exerted by the wind turbines. Here, U_h is the average wind speed at hub height, and c_t is the wind farm thrust coefficient defined as $c_t = \frac{\pi}{8}\frac{C_T}{S^2}$.

To close the system of equations, we need to determine U_h. Equation 11 approximates the geostrophic drag law (see [45]), providing a formula to estimate the friction velocity $u_{*\text{lo}}$ in the lower boundary layer. The geostrophic wind speed G is influenced by the Coriolis force, where $f' = 2\Omega \sin\theta$ is the Coriolis parameter, in which Ω denotes the rotational speed of the earth, and θ is the latitude, and the constant $A^* = 4$ at latitude 55°. We will define $f = f' e^{A^*}$[10].

$$u^*_{\text{lo}} = \frac{\kappa G}{\ln\left(\frac{G}{f' e^{A^*} z_{0,\text{lo}}}\right)} \tag{11}$$

$$U_h = \frac{G}{1 + \ln\left(\frac{G}{f \cdot h}\right)\sqrt{c_t + \left(\frac{\kappa}{\ln(h/z_{0,\text{lo}})}\right)^2}} \tag{12}$$

Equation 12 computes the mean wind speed U_h at hub height within the wind farm. This formulation considers the wind speed reduction due to wake effects as a function of c_t, the wind farm thrust coefficient, the height of the hub h and the geostrophic wind speed assuming a logarithmic wind profile.

Often, only the undisturbed mean wind speed at given heights is known for a specific site. This is the case in this work, where the unperturbed wind speed is retrieved from [6]. The geostrophic wind speed is then determined by setting $c_t = 0$ and solving Equation 12 for G.

1.3.4 Wind Resource and Production modeling

To estimate the wind farm power production, we need to model the convolution of the wind speed distribution with the power curve of the wind farm/turbine. We follow the approach presented in [43], combining a simple Weibull distribution model for the wind speed at a given height.

$$f(x;\lambda,k) = \begin{cases} \frac{k}{\lambda}\left(\frac{x}{\lambda}\right)^{k-1} e^{-\left(\frac{x}{\lambda}\right)^k} & \text{for } x \geq 0, \\ 0 & \text{for } x < 0 \end{cases} \tag{13}$$

[10] The nomenclature differs from that used by [45].

Equation 13 describes the Weibull probability density function, which is widely used to model wind speed distributions. Here, x represents the wind speed, k is the shape parameter, and λ is the scale parameter.

$$\begin{aligned} P_{WF,y} = &\int_{U_{in}}^{U_{out}} P(U) f(U;\lambda,k)\, dU = \\ =&\alpha \int_{U_{in}}^{U_r} U^3 f(U;\lambda,k)\, dU + \beta \int_{U_{in}}^{U_r} f(U;\lambda,k)\, dU + P_G \int_{U_r}^{U_{out}} f(U;\lambda,k)\, dU \end{aligned} \tag{14}$$

Equation 14 calculates the yearly energy production P_y from the wind turbine, integrating the turbine's power curve $P(U)$ over the range of operating wind speeds from U_{in} (cut-in speed) to U_{out} (cut-out speed), convoluted with the Weibull distribution of wind speeds of Equation 13.

$$\begin{aligned} P_{WF,y} =&\alpha\lambda^3 \left[\Gamma\left(\frac{3+k}{k}, \left(\frac{U_{in}}{\lambda}\right)^k\right) - \Gamma\left(\frac{3+k}{k}, \left(\frac{U_r}{\lambda}\right)^k\right)\right] + \\ &\beta\left(e^{-\left(\frac{U_{in}}{\lambda}\right)^k} - e^{-\left(\frac{U_r}{\lambda}\right)^k}\right) + P_G\left(e^{-\left(\frac{U_r}{\lambda}\right)^k} - e^{-\left(\frac{U_{out}}{\lambda}\right)^k}\right) \end{aligned} \tag{15}$$

Equation 15 gives a closed-form expression for the annual energy production of Equation 14, using the incomplete gamma function $\Gamma(,)$.

$$\begin{aligned} P_{WF,y} =&\alpha(\epsilon_1\lambda)^3 \left[\Gamma\left(\frac{3+k}{k}, \left(\frac{U_{in}}{\epsilon_1\lambda}\right)^k\right) - \Gamma\left(\frac{3+k}{k}, \left(\frac{U_r}{\epsilon_1\lambda}\right)^k\right)\right] + \\ &\beta\left(e^{-\left(\frac{U_{in}}{\epsilon_1\lambda}\right)^k} - e^{-\left(\frac{U_r}{\epsilon_1\lambda}\right)^k}\right) + P_G\left(e^{-\left(\frac{U_r}{\epsilon_2(U_r)\lambda}\right)^k} - e^{-\left(\frac{U_{out}}{\epsilon_2(U_{out})\lambda}\right)^k}\right) \end{aligned} \tag{16}$$

Equation 16 modifies Equation 15 to include the effect of changing the velocity profile of the Atmospheric Boundary Layer by the added roughness and shear caused by the infinite wind farm, which refines the calculation by adjusting the wind speed scale parameter λ for the reduction caused by wakes, using ϵ_1 and ϵ_2 which are functions of the wake decay factor and turbine spacing. This equation further nuances the wake effect by varying the scale factor depending on the wind speed, providing more accurate predictions of turbine performance under real conditions.

$$\begin{aligned} \epsilon_1 =&\frac{1+\frac{\gamma}{\delta}}{1+\frac{\gamma}{\kappa}\sqrt{\frac{\pi C_{T,\text{rated}}}{8S^2} + \left(\frac{\kappa}{\delta}\right)^2}} \\ \epsilon_{2_{(U_\epsilon)}} =&\frac{1+\frac{\gamma}{\delta}}{1+\frac{\gamma}{\kappa}\sqrt{\frac{\pi C_{T,\text{rated}}}{8S^2}\left(U_r/U_\epsilon\right)^{3.2} + \left(\frac{\kappa}{\delta}\right)^2}} \end{aligned} \tag{17}$$

Equation 17 defines ϵ_1 and ϵ_2, the adjustment factors for the wind speed scale parameter within the wind farm. These factors account change in the velocity profile as

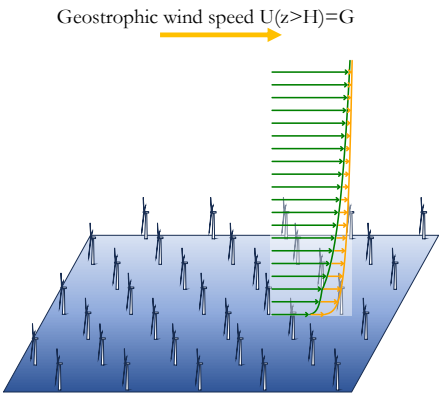

Fig. 3 Representation of the velocity profile of the Atmospheric Boundary Layer (ABL) inside the wind farm (green) and in the absence of the wind farm (orange), up to the geostrophic wind speed.

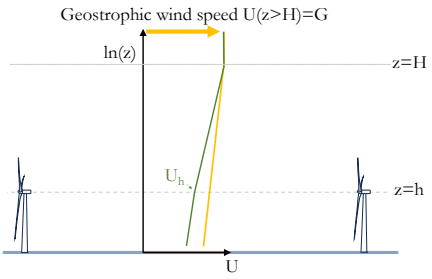

Fig. 4 Log-scale representation of the velocity profile of the ABL inside the wind farm (green) and in the absence of the wind farm (orange), up to the geostrophic wind speed. Scales are not proportional.

function of loading for below rated and at cut-out. The parameters γ and δ are defined by:

$$\gamma = \ln\left(\frac{G}{fh}\right), \quad \delta = \ln\left(\frac{h}{z_{0,\mathrm{lo}}}\right) \tag{18}$$

1.3.5 Finite wind farm effect

The previous equations represent the solution for an infinite wind farm. However, for a finite wind farm, the first rows of wind turbines will experience wind conditions between unperturbed flow and fully developed wind farm. The work of [43] presented a formulation that considers that a certain quantity of wind turbines at/close to the edge of the wind farm experience unperturbed flow, assuming a squared wind farm. In this work, the number of edge wind turbines experiencing unperturbed wind is defined as $M_{rows} * M_{turbines}$, where the first represents a depth of rows into the wind farm and the second represents the number of turbines experiencing unperturbed wind.

1.4 Definition of the Wind Farm Wind Factor

The description of the wind farm in our model is characterized by several variables: some define the shape and dimensions of the wind farm (e.g., number of turbines), others the local wind resource (e.g., shape and scale factors of the wind speed distribution), others the properties of the wind turbines, and still others the load that the wind farm exerts on the atmosphere. The diverse range of variables makes each wind farm unique. Furthermore, these variables collectively influence the wind farm's capacity factor. Consequently, the problem manifests as multidimensional. However, for simplicity, we aim to transform it into a predominantly *one-dimensional* problem, where the capacity factor is principally determined by a single variable. Upon analysis of the integral for the capacity factor of Equation 16, we find that it is primarily

dictated by a ratio of the rated wind speed of the turbine to the average wind speed perceived by the wind farm, which includes the deceleration effect of the atmospheric boundary layer profile. We define this ratio as the *Wind Farm Wind Factor* ϕ_{WF}, expressed by Equation 19:

$$\phi_{WF} = \frac{U_r}{\overline{U}_\infty \epsilon_1} \tag{19}$$

where U_r is the rated wind speed of the turbine model used in the wind farm; $\overline{U}_\infty$ is the average speed of the unperturbed wind at the location of the wind farm (in the absence of the wind farm), at hub height. Based on the Weibull distribution, it is defined as

$$\overline{U}_\infty = \lambda \cdot \Gamma\left(\frac{1+k}{k}\right) \tag{20}$$

and $\epsilon = \epsilon_1$ is the wind speed reduction factor.

We can define the capacity factor of the wind farm as

$$C_F = \frac{P_{WF,y}}{P_G} \tag{21}$$

We can define a limit for maximum capacity factor by assuming $U_{in} = 0$ and $U_{out} = \infty$. Equation 16 then can be rewritten for the limit capacity factor

$$C_{F_{max}} = {\phi_{WF}}^{-3}\Gamma\left(\frac{1+k}{k}\right)^{-3}\left[1-\Gamma\left(\frac{3+k}{k}, {\phi_{WF}}^{k}\Gamma\left(\frac{1+k}{k}\right)^{k}\right)\right] + e^{-\phi_{WF}^{k}\Gamma\left(\frac{1+k}{k}\right)^{k}} \tag{22}$$

Equation 22 shows that the maximum capacity factor is then just a function of the Wind Farm Wind Factor and the shape factor of the Weibull distribution.

2 Validation of the model with real wind farm data

2.1 Validation of model with wind farm data

In this section, we validate the estimates of the model against real wind farm data of the capacity factor. Figure 6 presents the capacity factor estimated by the model vs. capacity factor from real wind farm data. It is important to notice that the model estimates the capacity factor assuming only wind-farm aerodynamic losses, without any operational losses. The wind farm data is the reported energy delivered to the system, which includes operational losses due to availability, transmission losses, maintenance, failures, grid availability, etc. These losses are often estimated to be in average 10% of the potential energy production. We can see in Figure 6 that almost all the real data values are between 85% and 95% of the values estimated by the model (average 89%), which can be explained by the aforementioned average 10% operational losses. A linear regression of the points in the figure of the form $y = 0.89x$ will have a coefficient of determination $R^2 = 0.87$.

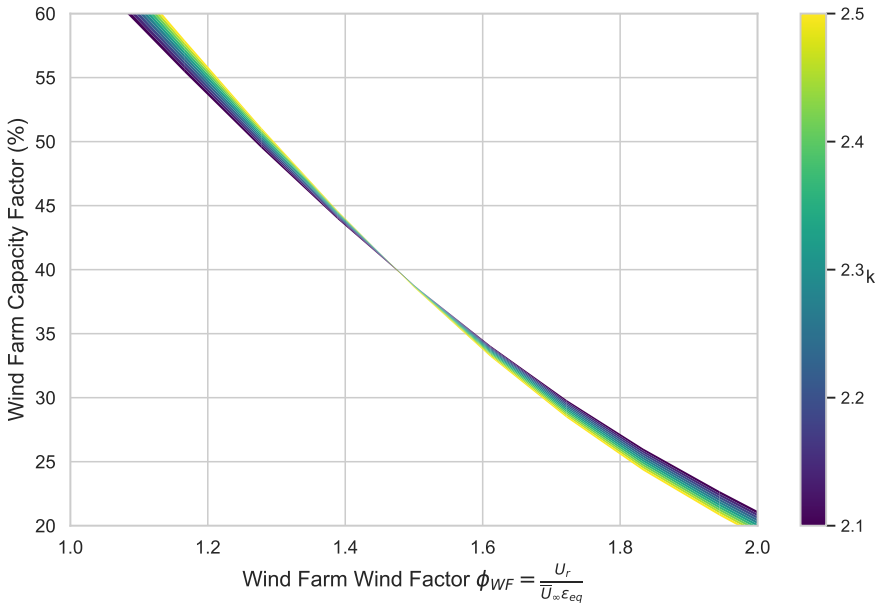

Fig. 5 limit of the capacity factor $C_{F_{max}}$ as a function of Wind Farm Wind Factor $\phi_{WF} = \frac{U_r}{U_\infty \epsilon_1}$ and the shape factor k of the Weibull distribution of the wind speed (color range).

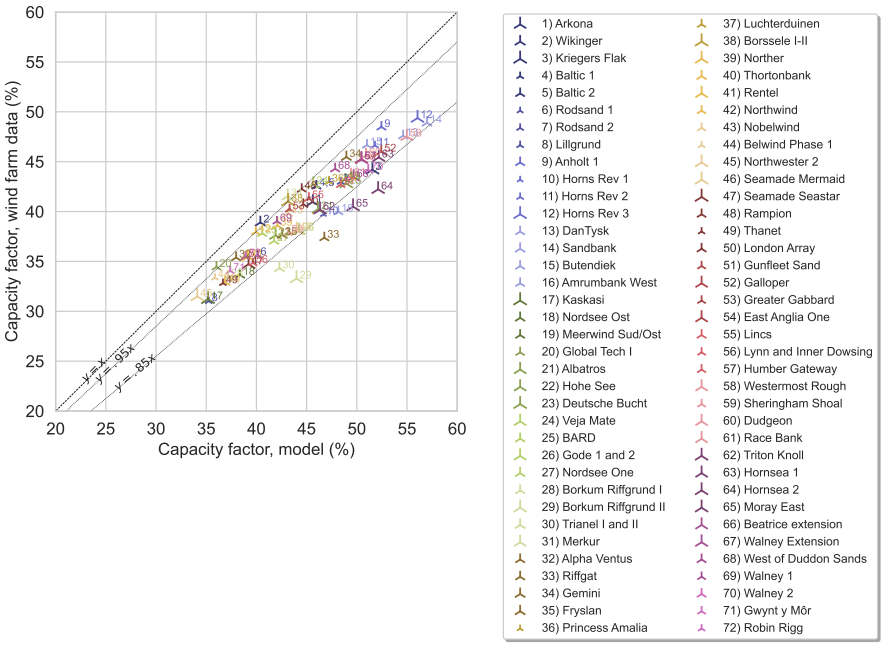

Fig. 6 Capacity factor estimated by the model vs. capacity factor from real wind farm data. Lines show 100%, 95% and 85% relations.

2.2 Validation of the Theoretical Limit for the Capacity Factor

Figure 7 presents the relationship between Wind Farm Wind Factor $\phi_{WF} = \frac{U_r}{\overline{U}_\infty \epsilon_{eq}}$ and Wind Farm Capacity Factor CF (%). The data points represent the individual wind farms. The theoretical-limit line for $k_w = 2.4$ and the theoretical-limit line accounting for 10% losses are also shown.

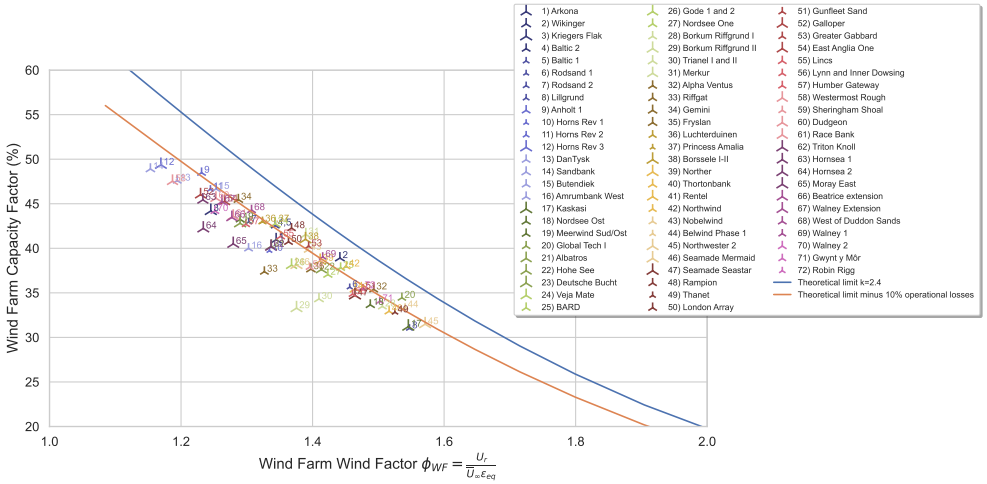

Fig. 7 Relationship between Wind Farm Wind Factor $\phi_{WF} = \frac{U_r}{\overline{U}_\infty \epsilon_{eq}}$ and Wind Farm Capacity Factor CF (%). The data points represent the individual wind farms. The theoretical-limit line for $k_w = 2.4$ and the theoretical-limit line accounting for 10% losses are also shown.

References

[1] Borrmann, R., Rehfeldt, K., Wallasch, A.-K., Lüers, S.: Capacity Densities of European Offshore Wind Farms. Deutsche WindGuard GmbH, Varel, Germany. Report conducted for the Federal Maritime and Hydrographic Agency under the Baltic LINes project (2018)

[2] Belgian Offshore Platform: Offshore Wind Farm Projects in Belgium. https://www.belgianoffshoreplatform.be/en/projects/. Accessed on: April 18, 2024 (2020)

[3] Vattenfall: Sandbank Power Plant. https://powerplants.vattenfall.com/sandbank/. Accessed: 2024-04-14 (2024)

[4] Power Technology: Power Technology Website. https://www.power-technology.com/. Accessed: 2024-04-14 (2024)

[5] Nordsee One GmbH: Nordsee One Offshore Wind Farm. https://www.nordseeone.com/. Accessed: 2024-04-14 (2024)

[6] Technical University of Denmark: Global Wind Atlas. https://globalwindatlas.info/en. Accessed: 2024-04-14 (2024)

[7] Sørensen, J., Larsen, G., Cazin-Bourguignon, A.: Production and cost assessment of offshore wind power in the north sea, vol. 1934. IOP Publishing, ??? (2021). https://doi.org/10.1088/1742-6596/1934/1/012019 . Wake Conference 2021 ; Conference date: 15-06-2021 Through 17-06-2021

[8] 4C Offshore: Offshore Wind Farms Map. Online. Accessed: 2024-04-21 (2024). https://map.4coffshore.com/offshorewind/

[9] Fraunhofer Institute for Solar Energy Systems ISE: Energy Charts for Germany. Accessed: April 3, 2024 (2024). https://energy-charts.info/index.html?l=en&c=DE

[10] Iberdrola: 2019 Annual Report. https://www.iberdrola.com/shareholders-investors/operational-financial-information/results. Accessed: 2024-04-05 (2019)

[11] Iberdrola: 2021 Annual Report. https://www.iberdrola.com/shareholders-investors/operational-financial-information/results. Accessed: 2024-04-05 (2021)

[12] Iberdrola: 2023 Annual Report. https://www.iberdrola.com/shareholders-investors/operational-financial-information/results. Accessed: 2024-04-05 (2023)

[13] Danish Energy Agency: Data Overview of the Energy Sector. Accessed: April 3, 2024 (2024). https://ens.dk/service/statistik-data-noegletal-og-kort/data-oversigt-over-energisektoren

[14] Vattenfall AB: Annual Report 2010. Accessed: 2024-04-13 (2010). https://group.vattenfall.com/siteassets/corporate/investors/annual-reports/2010/annual_report_2010.pdf

[15] Netztransparenz: EEG Annual Settlements 2000-2022. Accessed: April 3, 2024 (2024). https://www.netztransparenz.de/de-de/Erneuerbare-Energien-und-Umlagen/EEG/EEG-Abrechnungen/EEG-Jahresabrechnungen/EEG-Jahresabrechnungen-2022-2000

[16] ewz (Deutschland) GmbH: Annual Report 2018. Available at https://www.ewz.ch/en/about-ewz/portrait/company/annual-and-sustainability-report.html. Accessed: April 3, 2024 (2018)

[17] ewz (Deutschland) GmbH: Annual Report 2019. Available at https://www.ewz.ch/en/about-ewz/portrait/company/annual-and-sustainability-report.html. Accessed: April 3, 2024 (2019)

[18] ewz (Deutschland) GmbH: Annual Report 2020. Available at https://www.ewz.ch/en/about-ewz/portrait/company/annual-and-sustainability-report.html. Accessed: April 3, 2024 (2020)

[19] ewz (Deutschland) GmbH: Annual Report 2021. Available at https://www.ewz.ch/en/about-ewz/portrait/company/annual-and-sustainability-report.html. Accessed: April 3, 2024 (2021)

[20] Northland Power: 2019 annual report. Annual report, Northland Power (2019). Accessed: 2024-04-05. https://www.northlandpower.com/en/investor-centre/corporate-reports.aspx

[21] Northland Power: 2020 annual report. Annual report, Northland Power (2020). Accessed: 2024-04-05. https://www.northlandpower.com/en/investor-centre/corporate-reports.aspx

[22] Northland Power: 2021 annual report. Annual report, Northland Power (2021). Accessed: 2024-04-05. https://www.northlandpower.com/en/investor-centre/corporate-reports.aspx

[23] Northland Power: 2022 annual report. Annual report, Northland Power (2022). Accessed: 2024-04-05. https://www.northlandpower.com/en/investor-centre/corporate-reports.aspx

[24] Northland Power: 2023 annual report. Annual report, Northland Power (2023). Accessed: 2024-04-05. https://www.northlandpower.com/en/investor-centre/corporate-reports.aspx

[25] GmbH, V.M.O.P.: Sustainability Report 2022. Deutscher Nachhaltigkeitskodex (DNK). Accessed: 2024-04-05 (2022)

[26] Trianel GmbH: Annual and Sustainability Report 2020. Available at https://www.trianel.com/en/company/facts-and-figures/annual-reports. Accessed: April 3, 2024 (2020)

[27] Trianel GmbH: Annual and Sustainability Report 2021. Available at https://www.trianel.com/en/company/facts-and-figures/annual-reports. Accessed: April 3, 2024 (2021)

[28] Trianel GmbH: Annual and Sustainability Report 2022. Available at https://www.trianel.com/en/company/facts-and-figures/annual-reports. Accessed: April 3, 2024 (2022)

[29] The Renewables Infrastructure Group Limited: Investors Reports and Publications 2020. Available at https://www.trig-ltd.com/investors/reports-and-publications/?classification=results&investors-year=2020. Accessed: April 3, 2024 (2020)

[30] The Renewables Infrastructure Group Limited: Investors Reports and Publications 2021. Available at https://www.trig-ltd.com/investors/reports-and-publications/?classification=results&investors-year=2021. Accessed: April 3, 2024 (2021)

[31] The Renewables Infrastructure Group Limited: Investors Reports and Publications 2022. Available at https://www.trig-ltd.com/investors/reports-and-publications/?classification=results&investors-year=2022. Accessed: April 3, 2024 (2022)

[32] The Renewables Infrastructure Group Limited: Investors Reports and Publications 2023. Available at https://www.trig-ltd.com/investors/reports-and-publications/?classification=results&investors-year=2023. Accessed: April 3, 2024 (2023)

[33] Windpark Fryslân: Windpark Fryslân. Available at https://www.windparkfryslan.nl/. Accessed: April 3, 2024 (2024)

[34] Eneco: Annual Report 2016. Available at https://www.eneco.nl/en/about-us/news-and-figures/finance/reports/. Accessed: April 3, 2024 (2016)

[35] Eneco: Annual Report 2017. Available at https://www.eneco.nl/en/about-us/news-and-figures/finance/reports/. Accessed: April 3, 2024 (2017)

[36] Eneco: Annual Report 2018. Available at https://www.eneco.nl/en/about-us/news-and-figures/finance/reports/. Accessed: April 3, 2024 (2018)

[37] Office of Gas and Electricity Markets (Ofgem): Renewables and Combined Heat and Power Register. Accessed: April 3, 2024 (2024). https://renewablesandchp.ofgem.gov.uk/

[38] Ørsted: Annual Report 2023. https://via.ritzau.dk/ir-files/13560592/8204/12529/%C3%98rsted%20annual%20report%202023.pdf. Accessed: April 3, 2024 (2023). https://via.ritzau.dk/ir-files/13560592/8204/12529/%C3%98rsted%20annual%20report%202023.pdf

[39] Ørsted: Annual Report for 2023 - Strong Underlying Results. https://orsted.com/en/company-announcement-list/2024/02/annual-report-for-2023--strong-underlying-results--82041. Accessed: April 3, 2024 (2023). https://orsted.com/en/company-announcement-list/2024/02/annual-report-for-2023--strong-underlying-results--82041

[40] Ørsted: Annual Reporting 2021. https://orsted.com/en/investors/ir-material/annual-reporting-2021. Accessed: April 3, 2024 (2021). https://orsted.com/en/investors/ir-material/annual-reporting-2021

[41] Ørsted: Annual Report 2021. https://orstedcdn.azureedge.net/-/media/annual2021/annual-report-2021.pdf?rev=9d4904ddf4c44594adab627f7e4c62be&hash=058C4C670D1172FAF9007236371100D2. Accessed: April 3, 2024 (2021). https://orstedcdn.azureedge.net/-/media/annual2021/annual-report-2021.pdf?rev=9d4904ddf4c44594adab627f7e4c62be&hash=058C4C670D1172FAF9007236371100D2

[42] Ørsted: Ørsted completes partnership with Norges Bank Investment Management on Borssele 1 & 2. https://orsted.com/en/media/news/2021/05/419222030612334. Accessed: April 3, 2024 (2021). https://orsted.com/en/media/news/2021/05/419222030612334

[43] Sørensen, J.N., Larsen, G.C.: A Minimalistic Prediction Model to Determine Energy Production and Costs of Offshore Wind Farms. Energies **14**(2), 448 (2021) https://doi.org/10.3390/en14020448 . Number: 2 Publisher: Multidisciplinary Digital Publishing Institute. Accessed 2023-06-21

[44] Sørensen, J.N., Larsen, G.C., Cazin-Bourguignon, A.: Production and Cost Assessment of Offshore Wind Power in the North Sea. Journal of Physics: Conference Series **1934**(1), 012019 (2021) https://doi.org/10.1088/1742-6596/1934/1/012019 . Accessed 2023-06-30

[45] Frandsen, S.T.: Turbulence and turbulence-generated structural loading in wind turbine clusters. Doctoral thesis (2007). ISBN: 9788755034587 Publication Title: Turbulence and turbulence-generated structural loading in wind turbine clusters

[46] Templin, R.J.: An estimate of the interaction of windmills in widespread arrays. Technical report, [object Object] (December 1974). https://doi.org/10.4224/21270260 . Artwork Size: 29 p. https://nrc-publications.canada.ca/eng/view/object/?id=94d3fbff-cb95-4967-8926-ebb4494d1578 Accessed 2024-04-21

[47] Frandsen, S.: On the wind speed reduction in the center of large clusters of wind turbines. Journal of Wind Engineering and Industrial Aerodynamics **39**(1), 251–265 (1992) https://doi.org/10.1016/0167-6105(92)90551-K . Accessed 2024-04-24